Published in final edited form as:
Cell Metab. 2014 November 4; 20(5): 813–826. doi:10.1016/j.cmet.2014.09.016.

Reducing Macrophage Proteoglycan Sulfation increases Atherosclerosis and Obesity through Enhanced Type I Interferon Signaling

Philip L.S.M. Gordts[1], **Erin Foley**[1,2], **Roger Lawrence**[1], **Risha Sinha**[1], **Carlos Lameda-Diaz**[1], **Liwen Deng**[1], **Ryan Nock**[1], **Christopher K. Glass**[1,3], **Ayca Erbilgin**[4], **Aldons J. Lusis**[4], **Joseph L. Witztum**[3], and **Jeffrey D. Esko**[1,2,*]

[1]Department of Cellular and Molecular Medicine, University of California, San Diego, La Jolla, California 92093

[2]Biomedical Sciences Graduate Program, University of California, San Diego, La Jolla, California 92093

[3]Department of Medicine, University of California, San Diego, La Jolla, California 92093

[4]Department of Cardiology, University of California, Los Angeles, Los Angeles, California 90095

Summary

Heparan sulfate proteoglycans (HSPGs) are an important constituent of the macrophage glycocalyx and extracellular microenvironment. To examine their role in atherogenesis, we inactivated the biosynthetic gene *N*-acetylglucosamine *N*-deacetylase-N-sulfotransferase 1 (*Ndst1*) in macrophages and crossbred the strain to $Ldlr^{-/-}$ mice. When placed on an atherogenic diet, $Ldlr^{-/-}Ndst1^{f/f}LysMCre^{+}$ mice had increased atherosclerotic plaque area and volume compared to $Ldlr^{-/-}$ mice. Diminished sulfation of heparan sulfate resulted in enhanced chemokine expression, increased macrophages in plaques, increased expression of ACAT2, a key enzyme in cholesterol ester storage, and increased foam cell conversion. Motif analysis of promoters of up-regulated genes suggested increased Type I Interferon signaling, which was confirmed by elevation of STAT1 phosphorylation induced by IFN-β. The pro-inflammatory macrophages derived from $Ndst1^{f/f}LysMCre^{+}$ mice also sensitized the animals to diet-induced obesity. We propose that macrophage HSPGs control basal activation of macrophages by maintaining Type I interferon reception in a quiescent state through sequestration of IFN-β.

*Correspondence: Jeffrey D. Esko, Department of Cellular and Molecular Medicine, University of California, San Diego, La Jolla, CA 92093-0687, Ph: 858/822-1100, FAX: 858/534-5611, jesko@ucsd.edu.

Introduction

Cardiovascular disease (CVD) is the leading cause of death globally, primarily as a result of complications of atherosclerosis. The complex pathology of atherosclerosis is characterized by the accumulation of lipids, inflammatory cells and fibrous elements in large and medium-sized arteries (Swirski and Nahrendorf, 2013). According to the “response-to-retention” model, focal infiltration and retention of apolipoprotein B (apoB)-containing lipoproteins, such as low density lipoproteins (LDL), lipoprotein (a) and triglyceride-rich remnant particles (TRLs), in the subendothelial matrix of the tunica intima of arteries at atherosclerosis-prone sites initiates atherogenesis (Tabas et al., 2007). Subsequent oxidation, lipolysis, proteolysis and further aggregation of trapped LDL particles contribute to a chronic inflammatory response characterized by monocyte and T-cell migration into the intima. Monocytes entering the plaque differentiate into macrophages and the expression of scavenger receptors results in internalization of modified lipoprotein particles. Lesion macrophages proliferate, accumulate massive amounts of cholesterol and become lipid droplet-loaded “foam cells”, resulting in their retention in the lesion (Robbins et al., 2013; Witztum and Lichtman, 2014).

Proteoglycans consist of a protein core and one or more covalently attached glycosaminoglycan (GAG) chains. Studies of human diseases and model organisms, have demonstrated the importance of proteoglycans in development and physiology (Sarrazin et al., 2011). Proteoglycans in the arterial wall help establish the architecture of the vessel and play roles in smooth muscle cell and endothelial cell proliferation (Wight, 1989). They also retain lipoproteins in the arterial wall via interaction of apoB and possibly other apolipoproteins with the negatively charged sulfate groups of the GAG chains (Tabas et al., 2007).

Little is known about the in vivo contribution of macrophage-derived proteoglycans to the development and progression of atherosclerosis. In vitro experiments have shown that lesion-derived macrophages produce pro-retentive proteoglycans and enhance LDL aggregation (Maor et al., 2000). Recently, we showed that the heparan sulfate proteoglycan (HSPG) syndecan-1 mediates uptake and clearance of triglyceride-rich lipoproteins in hepatocytes (Stanford et al., 2009). Conceivably, macrophage proteoglycans might act in a similar way, facilitating uptake and clearance of lipoprotein particles, possibly contributing to foam cell formation in the artery.

In this study we determined the impact on atherosclerosis of altering the structure of heparan sulfate in monocytes/macrophages by inactivation of a heparan sulfate biosynthetic enzyme (*Ndst1*) selectively in the myeloid lineage. Contrary to expectations, the inactivation of *Ndst1* exacerbated atherosclerosis in mice deficient in LDL receptors ($Ldlr^{-/-}$). Analysis of inflammatory markers revealed that macrophages from the mutant were in an activated state, leading to secretion of proinflammatory cytokines and enhanced macrophage infiltration, foam cell conversion and development of atherosclerotic lesions. The pro-inflammatory shift also increased diet-induced obesity. We show that macrophage HSPGs regulate the inflammatory state in a cell autonomous fashion by maintaining Type I interferon (IFN) reception in a quiescent state through sequestration of IFN-β. Together, the data suggest that

HSPGs are important in regulating the threshold for Type I interferon stimulation of macrophages.

Results

Myeloid-specific *Ndst1* gene disruption alters heparan sulfate in macrophages

Heparan sulfate (HS) assembly occurs by the copolymerization of *N*-acetylglucosamine (GlcNAc) and glucuronic acid (GlcA) residues, followed by a series of processing reactions catalyzed by several sulfotransferases, an epimerase and cell surface sulfatases. Of the four Ndst isozymes that have been described, only *Ndst1* and *Ndst2* are expressed in macrophages (Fig. 1A). In order to determine the impact of altering Ndst1 expression, we crossbred mice bearing a conditional loxP-flanked ("floxed") allele of *Ndst1* (*Ndst1*$^{f/f}$) to transgenic mice expressing the bacterial Cre recombinase under control of the lysozyme 2 promoter (*LysMCre*) to drive inactivation of the gene in myeloid cells. Quantitative PCR (qPCR) analysis of mRNA collected from bone marrow-derived macrophages (BMDMs) from *Ndst1*$^{f/f}$*LysMCre*$^{+}$ mice showed almost complete inactivation (~98%) of *Ndst1* expression (Fig. 1A), without any compensation by *Ndst2–4*.

Macrophages express a relatively highly sulfated HS, rich in trisulfated and disulfated disaccharides (D2S6 and D2S0; Suppl. Fig. 1). However, inactivation of *Ndst1* in macrophages induced relatively modest changes in overall HS composition compared to other cell types (Supp. Fig. 1) (MacArthur et al., 2007), decreasing the level of N-sulfation from 53 N-sulfoglucosamine residues/100 disaccharides in wild-type macrophages to 44/100 disaccharides in the mutant (~15% reduction; Fig. 1B), with a corresponding increase in *N*-acetylglucosamine residues from 47/100 disaccharides in the wild-type to 55/100 disaccharides in the mutant. The remaining *N*-sulfoglucosamine residues arose presumably from the action of Ndst2 (Fig. 1A). Due to coupling of *N*-sulfation to downstream biosynthetic reactions, the number of 2-*O*-sulfate groups located on the uronic acids decreased from 46/100 disaccharides in the wild-type to 39/100 disaccharides in the mutant (~14%) and the extent of glucosamine 6-O-sulfation decreased from 38 sulfates/100 disaccharides in the wild-type to 34/100 disaccharides in the mutant (~10%). The modest change in composition nevertheless significantly diminished binding of HS-binding ligands, such as FGF2 (~40%, Fig. 1C).

Myeloid-specific *Ndst1* gene disruption Increases atherosclerosis

To examine the impact of altering macrophage HS on atherosclerosis, we bred *Ndst1*$^{f/f}$*LysMCre*$^{+}$ mice onto an *Ldlr*$^{-/-}$ background. In preliminary studies, we found that feeding a high-fat, high-cholesterol (HFC) diet to the male mice led to greater weight gain than in female mice. Therefore, to avoid complications of differential weight gain, we fed female animals a HFC diet for up to 12 weeks. Total cholesterol and triglyceride levels did not differ between *Ldlr*$^{-/-}$*Ndst1*$^{f/f}$*LysMCre*$^{+}$ and *Ldlr*$^{-/-}$*Ndst1*$^{f/f}$*LysMCre*$^{-}$ mice prior to placing the animals on the diet (Fig. 2A–B). Plasma triglycerides and cholesterol progressively increased to the same extent in both strains on the HFC diet. FPLC analysis of plasma taken after 12-weeks demonstrated equivalent accumulation of chylomicron/VLDL triglycerides and chylomicron/VLDL and IDL/LDL cholesterol in both strains, while HDL

cholesterol levels were unchanged (Fig. 2C–D). No difference in body weight was observed between *Ldlr*$^{-/-}$*Ndst1*$^{f/f}$*LysMCre*$^{-}$ and *Ldlr*$^{-/-}$*Ndst1*$^{f/f}$*LysMCre*$^{+}$ (24.2 ± 0.8 g [n=14] versus 25.0 ± 1.1 g [n=15]) mice at the end of the feeding period. Glucose homeostasis between the groups was similar based on their fasting glucose and insulin levels, although there was a trend towards higher glucose and lower insulin in the mutant (Fig. 2E–F). Glucose tolerance and insulin tolerance were comparable (Fig. 2G–H).

En face analysis of atherosclerosis in the aorta showed plaque formation restricted to the aortic root and arch in both strains (Fig. 2I). However, inactivation of *Ndst1* caused a two-fold increase in plaque surface area in *Ldlr*$^{-/-}$*Ndst1*$^{f/f}$*LysMCre*$^{+}$ mice compared to *Ldlr*$^{-/-}$*Ndst1*$^{f/f}$*LysMCre*$^{-}$ controls expressed either as a percentage of total surface area and by absolute plaque area (Fig. 2J). A similar significant increase was observed in male mice (Supp. Fig. 1B–C). Aortic root cross-sectional analysis confirmed that plaque volume in *Ldlr*$^{-/-}$*Ndst1*$^{f/f}$*LysMCre*$^{+}$ mice increased as well (Fig. 2K–L). Visual inspection of van Gieson stained cross sections of lesions at the aortic root strongly suggested that plaques from *Ldlr*$^{-/-}$*Ndst1*$^{f/f}$*LysMCre*$^{+}$ mice had larger necrotic cores (Fig 2M), which was confirmed by image quantitation (Fig. 2N), suggesting that the lesions were more advanced compared to those in control mice. Lesions from *Ldlr*$^{-/-}$*Ndst1*$^{f/f}$*LysMCre*$^{+}$ mice also had a significantly higher macrophage content compared to lesions from control mice (40% of lesion area in the mutant vs. 25% in the wild-type; $P<0.001$) (Fig. 2M lower panel and Fig. 2O), but T-cell infiltration was not elevated (Supp. Fig. 1D–F). The proliferating and apoptotic cell content in the lesions was similar between the groups as well (Supp. Fig. 1G–J).

ApoE bound to HSPGs controls proliferation of hematopoietic stem and multipotential progenitor cells in the bone marrow, monocytosis and monocyte accumulation in atherosclerotic lesions in mice (Murphy et al., 2011). *Ldlr*$^{-/-}$*Ndst1*$^{f/f}$*LysMCre*$^{+}$ and *Ldlr*$^{-/-}$*Ndst1*$^{f/f}$*LysMCre*$^{-}$ mice showed no difference in monocyte (Fig. 2P) or neutrophil counts (Fig. 2Q). Also plasma lymphocyte counts (Supp. Fig. 1I) and total white blood cell counts (Supp. Fig. 1J) did not differ.

These findings suggest that altering macrophage proteoglycan sulfation exacerbates atherosclerosis, enhances the number of macrophages in the lesion and lesion composition, but it does not affect plasma lipoproteins, infiltration of neutrophils and T-cells, or plasma myeloid or lymphocyte counts.

Macrophage proteoglycans modulate foam cell formation

Macrophage syndecan-4, a type of HSPG, has been implicated in foam cell conversion in vitro (Boyanovsky et al., 2009). To test if inactivation of Ndst1, which affects sulfation of all HSPGs in targeted cells, also reduced foam cell conversion, we elicited peritoneal macrophages in *Ldlr*$^{-/-}$*Ndst1*$^{f/f}$*LysMCre*$^{+}$ and *Ldlr*$^{-/-}$*Ndst1*$^{f/f}$*LysMCre*$^{-}$ mice fed an HFC diet. In contrast to these earlier findings, macrophages isolated from *Ldlr*$^{-/-}$*Ndst1*$^{f/f}$*LysMCre*$^{+}$mice stained more intensely with Oil red O and accumulated significantly more cholesterol esters than *Ldlr*$^{-/-}$*Ndst1*$^{f/f}$*LysMCre*$^{-}$ macrophages (Fig. 3A–C). To examine foam cell conversion in vitro, bone marrow derived macrophages (BMDM) were isolated and challenged with normal LDL, aggregated LDL (agLDL) and oxidized

LDL (oxLDL). Incubation with agLDL dramatically induced cholesterol ester accumulation compared to the other lipoprotein preparations and occurred to a greater extent in macrophages derived from *Ndst1$^{f/f}$LysMCre^{+}* mice than control mice (Fig. 3D–E). Treatment of the cells with lipopolysaccharide enhanced further the extent of cholesterol ester accumulation in wild-type macrophages, but did not accentuate the elevation caused by altering HS (Fig. 3F). No gross changes were observed in free cholesterol levels between *Ndst1$^{f/f}$LysMCre^{+}* and *Ndst1$^{f/f}$LysMCre^{-}* macrophages (Supp. Fig. 2A–D). Macrophages from both male and female mutant mice responded similarly.

Incubation of BMDM for 1h with DiD-agLDL at 4°C or 37°C did not show any significant difference in binding or cell association (e.g. the sum of binding and uptake) between the two genotypes (Fig. 3G). Reverse cholesterol transport, as measured by efflux of ^{3}H-cholesterol to apolipoprotein AI or high density lipoproteins (HDL), was slightly decreased in *Ndst1$^{f/f}$LysMCre^{+}* macrophages compared to controls (Fig. 3H), but the difference did not reflect an alteration in HDL binding (Supp. Fig. 2E) or expression of cell surface ABCA1 transporters and apolipoprotein E (Supp. Fig. 2F–G). The small decrease in efflux of radioactive cholesterol did not correspond to any difference in total cholesterol ester loss measured chemically, suggesting that decreased efflux was not the cause for the accumulation of lipid in the mutant macrophages (Fig. 3I).

Ndst1-deficiency results in an inflammatory gene expression profile

To gain insight into the mechanism underlying the alterations in the mutant, we compared the transcriptome of BMDMs from *Ndst1$^{f/f}$LysMCre^{-}* and *Ndst1$^{f/f}$LysMCre^{+}*macrophages in basal growth medium (Fig. 4A). Increased expression of a relatively small set of genes occurred in the mutant, treated or untreated with agLDL, mostly in genes with functional annotations linked to immunity, defense and inflammatory response (Fig. 4B and Table S1). A comparable number of genes were decreased in expression, but these were linked to transmembrane signaling or apoptosis (Fig. 4C). qPCR analysis confirmed the enhanced expression of CCL2, CCL5, CCL7 and CCL8 (Fig. 4D). ELISA confirmed increased secretion of CCL5 and CCL7 (Fig. 4E–G). Other inflammatory genes were elevated as well, including TNFα, Ly6a, and IL10 (Fig. 4D). LPS treatment of macrophages greatly amplified the expression of these genes and diminished the differences in gene expression between mutant and wild-type seen under basal conditions, with the exception of CCL5 and IL10 (Supp. Fig. 3A). While IL10 is an anti-inflammatory cytokine, it is one of the most highly induced genes in classically activated macrophages following exposure to Toll-like Receptor ligands (Re and Strominger, 2004). Expression of other anti-inflammatory markers in mutant macrophages was either reduced or unaltered compared to wildtype (Supp. Fig 3B).

Several of these chemokines act as chemoattractants for monocytes, thus providing a plausible explanation for the enhanced content of macrophages in the atherosclerotic lesions (Fig. 2M and 2O). To test if similar changes in gene expression occurred *in vivo* we dissected plaques from the aortic arch and extracted mRNA for qPCR analysis, correcting transcript expression for macrophage content in the tissue (F4/80 expression). The results confirmed significant elevated expression of inflammatory genes (CCL2, CCL7, CCL8, TNF-α, and IL6) in the atherosclerotic plaques with the exception of CCL5 and IL-10 (Fig.

4I). These findings suggest that the accumulating lesion macrophages express inflammatory genes and are thus proinflammatory M1-like (Ly6c-hi) macrophages. To evaluate if monocyte recruitment was altered, we tagged Ly6c-hi monocytes with fluorescent beads (Tacke et al., 2007) and showed enhanced accumulation into lesions of *Ldlr*$^{-/-}$*Ndst1*$^{f/f}$*LysMCre*$^{+}$ mice compared to control mice (Fig. 2J–K).

ACAT2, an enzyme that converts cholesterol into cholesterol ester using long chain fatty acyl-coenzyme A, also was enhanced in *Ndst1*$^{f/f}$*LysMCre*$^{+}$ macrophages (Fig. 4D). Western blot analysis of ACAT1 and ACAT2 expression revealed that both enzymes were significantly increased in *Ndst1*$^{f/f}$*LysMCre*$^{+}$ macrophages (Supp. Fig. 3C). Interestingly, the increase in ACAT1 protein expression did not correlate with increased ACAT1 mRNA levels, except under conditions in which *Ndst1*$^{f/f}$*LysMCre*$^{+}$ BMDMs were stimulated with LPS (Supp. Fig. 3D). Incubation of macrophages with agLDL and the ACAT inhibitor (ACATi) Sandoz 58–035 blocked accumulation of cholesterol esters, normalizing the levels in the mutant to that seen in the wildtype (Fig. 4L). Treatment of BMDMs with chloroquine, which inhibits lysosomal degradation of LDL particles, also prevented cholesterol ester accumulation (Fig. 4L). Taken together, these findings suggest that elevated expression of both ACAT1 and ACAT2 in *Ndst1*$^{f/f}$*LysMCre*$^{+}$enhanced foam cell conversion.

Myeloid-specific *Ndst1* Gene disruption promotes diet-induced obesity

Given the activated state of macrophages in *Ndst1*$^{f/f}$*LysMCre*$^{+}$ mice, we wondered if the animals also might be susceptible to diet-induced obesity. Aged-matched male mice on a chow diet did not show any differences in body weight gain between the genotypes (Fig. 5A). However, when fed a high fat diet, *Ndst1*$^{f/f}$*LysMCre*$^{+}$ mice were consistently heavier, with a significant increase in the rate of weight gain after 6 weeks (Fig. 5B). The increased body weight gain of the mutant mice correlated with increased mass of white adipose tissue (WAT), brown adipose tissue (BAT) and the liver, whereas other organs such as muscle were unaffected (Fig. 5C). The diameter of the adipocytes in white adipose tissue increased as well, consistent with accumulation of lipid droplets (Fig. 5D). Histological analysis revealed that *Ndst1*$^{f/f}$*LysMCre*$^{+}$ mice exhibited increased lipid accumulation in liver, WAT, BAT and skeletal muscle (Fig. 5D–E).

The increase in weight gain in mutant mice fed a HFC diet was not associated with differences in food intake (Fig. 5F). Indirect calorimetry measurements at the end of HFC diet showed a trend towards reduced oxygen consumption and CO_2 production in *Ndst1*$^{f/f}$*LysMCre*$^{+}$ mice, which translated into a significant reduction in energy expenditure during the dark phase (Fig 5G–I). These changes were independent of alterations in respiratory exchange ratio (RER) or activity levels between both mouse groups (Fig. 5J–K).

The increase in weight gain on the HFC diet was associated with pronounced differences in glucose homeostasis between the groups. *Ndst1*$^{f/f}$*LysMCre*$^{+}$ mice had elevated fasting plasma glucose and NEFA (non-esterified fatty acid) levels and exhibited a pronounced hyperinsulinemia before and after glucose challenge (Fig. 5L–N). Reduced glucose and insulin tolerance indicated that *Ndst1*$^{f/f}$*LysMCre*$^{+}$ mice had developed severe type-2 diabetes compared to control mice on the high-fat diet (Fig. 5O–P).

The increase fat content in adipose tissue and liver also correlated with increased macrophage infiltration (F4/80 and CD11c+ cells, Fig. 6A–C). More F4/80 macrophages stained for CD11c, suggesting that the cells were in an activated state (Fig. 6D). Expression of inflammatory cytokines, CCL2, CCL5, CCL7, CCL8, TNF-α, and IL-6 was elevated as well (Fig. 6E–J), but changes in IL-10 expression were modest (Fig. 6K). Accumulation of pro-inflammatory macrophages in adipose tissue is a hallmark of obesity-associated inflammation, which exacerbates adipogenesis and lipid deposition in tissues (Jin et al., 2013). We found that the inflammation in BAT correlated with reduced expression of PRDM16, PGC-1 and Evolv3, all markers for BAT associated non-shivering thermogenesis (Fig. 6L). Thus, the macrophage status in the adipose tissue was similar to that observed in macrophages present in the atherosclerotic lesions and their accumulation in adipose tissues is consistent with enhanced diet-induced obesity in the *Ndst1*$^{f/f}$*LysMCre*$^{+}$ mice.

Macrophage proteoglycans regulate Type I interferon signaling via IFN-β

In search of a molecular mechanism to explain the increased inflammatory state of the macrophages in *Ndst1*$^{f/f}$*LysMCre*$^{+}$ mice, we analyzed promoter motifs of all of the genes that were expressed at higher levels in the transcriptome data sets. This analysis revealed that approximately 20% of the genes contain recognition motifs for Interferon Regulatory Factors (IRFs) and ISGF3, a complex of STAT1, STAT2 and IRF9 (Fig. 7A). These factors activate expression of genes involved in inflammation in response to Type I Interferon stimulation. Macrophages constitutively express a tonic (or basal) level of IFN-β (Gough et al., 2012), raising the possibility that macrophage proteoglycans modulate the activity of IFN-β and/or other members of the Type I interferon family. To test this possibility, we challenged macrophages from wild-type and *Ndst1*$^{f/f}$*LysMCre*$^{+}$mice with IFN-β and measured downstream phosphorylation of STAT1. Although we did not detect any difference in the baseline level of STAT1 phosphorylation, *Ndst1*$^{f/f}$*LysMCre*$^{+}$ macrophages responded more robustly to stimulation by exogenous IFN-β compared to control macrophages (Fig. 7B). Enzymatic treatment of wild-type macrophages with heparin lyase III, which degrades the HS chains on cell surface proteoglycans, provided a phenocopy of the mutant characterized by increased Stat1 phosphorylation in response to IFN-β (Fig. 7C). Treatment of mutant cells with heparin lyase III amplified their response to exogenous IFN-β as well, because the mutant macrophages make an undersulfated form of HS that remains susceptible to enzymatic digestion (Fig. 7D). Soluble heparin attenuated IFN-β mediated Stat-1 phosphorylation in wild-type macrophages in a dose-dependent fashion (Fig 7E–F). Stimulation of wild-type BMDMs with IFN-β increased expression of CCL5, CCL7, ACAT1 and ACAT2 (Fig. 76G–J), overall ACAT enzyme activity (Fig. 7K) and provoked foam cell formation in the presence of agLDL (Fig. 7L and Supp. Fig. 4A).

Type I IFNs signal through the receptors IFNAR1 and IFNAR2 (Gough et al., 2012). Treatment with an antibody against IFNAR1 reduced ACAT2 expression in *Ndst1*$^{f/f}$*LysMCre*$^{+}$ macrophages (Supp. Fig. 4D), indicating that the cells were undergoing basal Type I interferon activation in the absence of exogenous interferons. Cell surface expression of IFNAR1 and IFNAR2 did not differ between *Ndst1*$^{f/f}$*LysMCre*$^{+}$and control macrophages (Supp. Fig. 4B–C). Filter binding assays did not show interaction of macrophage-derived HS with soluble IFNAR1 and IFNAR2, alone or in complex with a

Type I IFN (Fig. 7M). In contrast, FGF-2 bound well to macrophage HS. IFNAR1 and IFNAR2 also did not bind to heparin-Sepharose (Supp. Fig. 4E).

We next surveyed a number of commercially available forms of Type I IFNs for their capacity to bind macrophage HS and found that IFN-β bound HS in a dose-dependent manner, whereas others such as IFN-α4 did not (Fig. 7N). We also found that IFN-β bound to HS from *Ndst1*$^{f/f}$*LysMCre*$^{+}$ macrophages less well compared to wild-type derived HS (Fig. 7O). Examination of the surface charge distribution deduced from the three-dimensional X-ray structure of IFN-β crystals (Senda et al., 1995) revealed a significant patch of positively charged amino acid residues consisting of six arginine and three lysine residues that could make up a potential binding site for HS (Fig. 7P). This hypothetical HS binding site (arrows) is not part of the IFN-β interface required for interaction with IFNAR1 (Fig. 7Q) (de Weerd et al., 2013).

Discussion

Based on previous studies showing that syndecan-1 in hepatocytes acts as an endocytic receptor for lipoproteins, we anticipated that the alteration in HS in macrophages would decrease the uptake of lipoproteins and protect the macrophage against foam cell conversion (MacArthur et al., 2007; Stanford et al., 2009). Other work suggested that reduction in sulfation might also diminish proteoglycan-mediated subendothelial retention of LDL particles in the artery wall and delay plaque progression (Tran-Lundmark et al., 2008). Thus, the increase in atherogenesis and foam cell conversion and enhanced disposition towards diet-induced obesity in *Ndst1*$^{f/f}$*LysMCre*$^{+}$ mice were unexpected phenotypes. Based on the data, macrophage HSPGs appear to play an atheroprotective role, by maintaining macrophages in a quiescent state under basal conditions through dampening the response to Type I interferons, such as IFN-β.

The increased Type-I interferon activation of the mutant macrophages leads to infiltration of pro-inflammatory M1-like or classically-activated macrophages in atherosclerotic lesions. In turn, the activated macrophages increase monocyte infiltration and macrophage cellularity in lesions (Moore et al., 2013; Tacke et al., 2007) and increase the propensity of macrophages to convert to foam cells. The increased inflammation and monocyte infiltration is most likely the driving factor for the increased susceptibility to atherosclerosis in the *Ldlr*$^{-/-}$*Ndst1*$^{f/f}$*LysMCre*$^{+}$ mice. It is important to note that the bead labeling method used in this study may inform on processes other than recruitment such as efferocytosis. It is also possible that fewer macrophages emigrate from the lesions in *Ldlr*$^{-/-}$*Ndst1*$^{f/f}$*LysMCre*$^{+}$ mice. Foam cell formation occurs through multiple mechanisms, which is why atherosclerosis progresses, albeit at slower rates, even when one or more pathways mediating foam cell formation are deleted. One prominent pathway is by uptake of modified LDL by macrophages (Witztum and Lichtman, 2014). Another prominent pathway is via uptake of agLDL (Frank and Fogelman, 1989) which in macrophages depends on the LDL receptor-Related Protein 1 and the formation of an extracellular acidic, hydrolytic compartment, the so-called lysosomal synapse (Haka et al., 2009). The changes in HSPGs composition induced in *Ndst1*$^{f/f}$*LysMCre*$^{+}$ mice did not affect binding or uptake of agLDL in macrophages, suggesting that lysosomal synapse-mediated uptake may not depend on

HSPGs. Previous studies have proposed a role for macrophage HSPGs in regulating apoE levels at the cell surface, thus modulating cholesterol efflux mediated by ApoE-HDL complexes (Murphy et al., 2011). However, cell surface apoE levels were similar in the mutant and efflux did not appear to be affected. We cannot exclude the possibility that more profound changes in HS might uncover effects on lipoprotein binding and uptake and cholesterol efflux, but alterations in these processes do not appear to contribute to the phenotype of the mutant mice used in this study.

ACAT2 was one of a small set of genes activated in *Ndst1*$^{f/f}$*LysMCre*$^{+}$macrophages and ACAT1 was elevated as well, suggesting that both isozymes contribute to foam cell conversion. We also show that IFN-β stimulation induced ACAT1 and ACAT2 expression and overall ACAT activity in macrophages. Previous studies showed that ACAT1 is the dominant isoform expressed in macrophages and that increased expression of ACAT1 in response to dexamethasone promotes foam cell formation (Yang et al., 2004). Based on enhanced ACAT activity in cell extracts and the inhibition of foam cell formation by an ACAT inhibitor, we propose that the increased inflammation in the *Ndst1*$^{f/f}$*LysMCre*$^{+}$ macrophages and consequent activation of ACAT contributes to the greater susceptibility of Ndst1-deficient macrophages to foam cell conversion. Increased IFN-β stimulation can also enhance survival of lipid-loaded macrophages by inhibiting apoptosis (Seimon et al., 2006), resulting in macrophage accumulation in atherosclerotic lesions. However, apoptotic genes were down-regulated in *Ndst1*$^{f/f}$*LysMCre*$^{+}$ macrophages, and we did not observe differences in apoptosis in atherosclerotic lesions.

Although atherosclerosis and obesity are very distinct conditions, they are both characterized by the accumulation M1-like macrophages and secretion of characteristic cytokines and chemokines (Jin et al., 2013). Priming of macrophages in *Ndst1*$^{f/f}$*LysMCre*$^{+}$ animals apparently suffices to promote increased macrophage infiltration and inflammation in aorta and adipose tissue, exacerbating atherosclerosis and obesity induced by a HFC diet. In the diet-induced obesity study this inflammation was most profound in BAT and associated with a reduction in energy expenditure and r BAT activity based on expression of the relevant genes. It is important to note that adipose tissue inflammation observed in the diet-induced obesity study was not observed in our atherosclerosis model (Supp. Fig 1M–N).

While IFN-γ has been shown to be important in M1 conversion and foam cell formation, less is known about the impact of Type I interferon signaling. Increased myeloid Type I IFN signaling promotes atherosclerosis in mice by stimulating macrophage recruitment to lesions (Goossens et al., 2010) and inhibition of IFN-β production can reduce adipose tissue inflammation in obese mice, consistent with the findings presented here (Abe et al., 2008). Recently IRF7, a master regulator of Type I interferon response, was found upregulated in liver and adipose tissue from obese mice compared to lean controls, indicating increased Type I interferon signaling (Wang et al., 2013). IRF7 knockout mice were resistant to diet-induced obesity, insulin resistance and inflammation. The IRF7 phenotype together with our data support that Type I interferon signaling is relevant and modulates diet-induced obesity, inflammation and its metabolic consequences. Consistent with this idea, inhibition of IFN-β

production by macrophages reduces adipose tissue inflammation in obese mice (Abe et al., 2008).

Type I interferons are typically expressed in response to viral or bacterial infection. However, macrophages constitutively express extremely low amounts of Type I IFNs, which nevertheless exert profound effects based on the ability of neutralizing antibodies to block activation and the lack of macrophage priming(i.e. setting the homeostatic inflammatory balance through tonic signaling) in mice with mutations in *Ifnar1* or *Ifnb* (Gough et al., 2012). Two Type I IFNs, IFN-κ and IFN-β, bind heparin (Nardelli et al., 2002), but the biological significance of this interaction has not been previously established. Based on the findings presented here, we propose that the capacity to bind HS provides a mechanism to retain these interferons near their site of secretion and to buffer their activity by preventing them from interacting with IFNAR1 and IFNAR2. The retention of heparin-binding IFNs also provides a pool of effectors that can be potentially released by alteration of cell surface HS.

A similar sulfation-dependent model has been proposed for regulation of Wnt and BMP signaling by HSPGs (Dhoot et al., 2001; Viviano et al., 2004). The interaction between Wnt and HS prevents Wnt signaling through frizzled receptors, but activation of extracellular sulfatases known as SULFs removes a small subset of sulfate groups located in highly sulfated domains in the chains, generating a soluble pool of Wnt and the initiation of Wnt signaling. It is conceivable that Sulfs or other HSPG modifying enzymes, such as matrix metalloproteases and heparanase, a heparan-degrading enzyme, might modulate the bioavailability of IFN-β in the macrophage microenvironment in a similar way. While we did no observe differences in heparanase expression in macrophages, increased heparanase expression has been linked to activation of innate immune cells, expression of inflammatory markers, such as CCL5, CCL2 and TNF-α, and plaque vulnerability (Blich et al., 2013; Osterholm et al., 2013).

Our results support a novel concept in innate immunity in which HSPGs are important for setting the basal activation threshold or activation status of macrophages through regulation of tonic Type I IFN signaling. Based on our results we propose a model wherein HSPGs determine the bioavailability of IFN-β for its receptors IFNAR1 and IFNAR2 on macrophages (Supp. Fig. 4E). Under resting conditions the highly sulfated HS produced by macrophages maintain Type I IFN reception in a quiescent state through sequestration of IFN-β. Reduction of cell-associated HSPG or HS composition increases the bioavailability of IFN-β for its receptors and activates macrophages by driving transcription of inflammatory genes. Additional research is warranted to link the exaggerated macrophage response to exogenous IFN-β ex vivo to the increase in atherosclerosis and obesity. The amazing sensitivity of this system to small changes in the degree of sulfation of HS induced by Ndst1 inactivation suggests that normal variation in the structure of HS could make some individuals more prone to macrophage priming and activation and downstream sequelae related to chronic inflammation (Shao et al., 2013; Wei et al., 2011). HS content and sulfation is decreased in advanced atherosclerotic lesions when compared to early lesions (Hollmann, 1989; Murata et al., 1997) and a recent study revealed a positive correlation for heparanase expression in human vulnerable plaques with expression of inflammatory

markers as CCL5, CCL2 and TNF-α (Osterholm et al., 2013). Our data warrant further analysis of macrophage HS and allelic variants of genes involved in HS metabolism in order to determine whether HSPG alterations have predictive value with respect to cardiovascular disease and obesity.

Experimental Procedures

Mice and Cell culture

Ndst1$^{f/f}$*LysMCre*$^{+}$ mice were generated by crossing *Ndst1*$^{f/f}$ mice to *LysMCre* transgenic mice (Clausen et al., 1999). *Ldlr*$^{-/-}$ mice were crossed with *Ndst1*$^{f/f}$*LysMCre*$^{+}$ mice to generate *Ldlr*$^{-/-}$*Ndst1*$^{f/f}$*LysMCre*$^{+}$ mice. Mice were fed *ad libitum* with water and standard rodent chow or a high fat/high cholesterol diet (TD.88137, Harlan Teklad). BMDM were isolated from 8 to 14-week old female mice. Peritoneal macrophages were harvested by peritoneal lavage 4 days after i.p. injection of 3 ml of thioglycollate (BD Biosciences).

Heparan sulfate purification and disaccharide analysis

BMDM were treated with a trypsin for 10 min at 37°C to release cell surface proteoglycans. Disaccharides were quantified by mass spectrometry as described (Lawrence et al., 2008).

Plasma lipids and lipoprotein distribution and blood cell analysis

Blood was obtained by cardiac puncture or via tail the vein. Plasma cholesterol and triglyceride levels (Sekesui, San Diego, CA, US) and NEFA levels (WAKO Diagnostics, VA, US) were measured by commercially available enzymatic kits.

Quantification of aortic atherosclerosis and monocyte labeling in vivo

Mice euthanized by isoflurane intoxication were perfused with 10 ml PBS. The heart and ascending aorta down to the iliac bifurcation were removed and stained for neutral lipids using Sudan IV. In addition, aortic root cross-sectional atherosclerosis lesion size was determined using ImageJ software. Classical Ly-6Clo monocytes were labeled in vivo and bead infiltration was analyzed as described (Tacke et al., 2007).

Immunohistochemistry

Mice euthanized by isoflurane intoxication were perfused with PBS and 10% formalin (Fisher, SF93-4). The upper part of the hearts were placed onto a tissue mold, covered in OCT (Tissue-Tek), and frozen. Serial 10-μm cryosections from similar parts of the aortic sinus were used for staining. All other tissues were embedded in paraffin. The extent of staining was measured with ImageJ software.

RNA analysis

Total RNA was isolated from homogenized tissue and cells in Trizol and purified using RNeasy columns (QIAGEN). qPCR (SYBR Green) analysis was performed on an Applied Biosystems 7300 Real-time PCR system (Invitrogen). Global gene expression was measured by microarray analysis using the Affymetrix HT_MG430A array. Data are uploaded to the

Gene Expression Omnibus and can be accessed via the following link: http://www.ncbi.nlm.nih.gov/geo/query/acc.cgi?token=sxkbymogflovlsn&acc=GSE51009.

Lipoprotein binding and uptake

Human LDL (density δ 1.019–1.063 g/mL) and HDL (density δ 1.063–1.21 g/mL) was isolated from plasma by buoyant density ultracentrifugation and quantified by BCA protein assay (Pierce).

Foam cell assay and reverse cholesterol transport

Macrophage cholesterol ester content was quantitated by the Amplex Red Cholesterol Assay Kit (Life Science Technologies, San Diego). Cholesterol ester content was calculated by subtracting free cholesterol from total cholesterol for each sample. Cholesterol efflux from BMDMs was performed as described (Nakaya et al., 2011).

Indirect Calorimetry

Mice were placed into Comprehensive Lab Animal Monitoring System (CLAMS; Columbus Instruments). Rates of O2 consumption (VO2; ml/kg/h) and CO2 production (VCO2) were measured for each chamber every 17 minutes throughout the study.

Glucose tolerance (GTT) and insulin tolerance test (ITT)

Mice were fasted for 5 hours. Blood samples were collected via tail vein bleeding immediately before and at 15, 30, 60, 90 and 120 min after oral glucose (2 mg/g body weight) gavage for GTT, after intraperitoneal injection of insulin (0.5U/g body weight) for ITT. Blood was immediately used for determination of glucose levels via the Accu-Chek® Aviva glucose monitoring system (Roche Applied Science GmbH, Mannheim, Germany). Insulin levels were determined via the ultra sensitive rat insulin ELISA kit (Chrystal Chem, Downers Grove, IL).

Nitrocellulose filter binding assay

Recombinant IFNAR1 (Life Science Technologies), IFNAR2, IFN-α4 and IFN-β (400 or 800 ng; PBL Interferon) were incubated with 10,000 counts of ^{35}S-labeled BMDM HS for 1 hr at 22 °C. The mixtures were applied to a prewashed nitrocellulose membrane to determine HS binding.

Stromal Vascular Fraction (SVF) isolation

Stromal vascular cells were prepared from collagenase-digested adipose tissue and FACS analysis of stromal vascular cells for macrophage content and subtypes was performed. The antibodies for surface staining were F4/80 (BM8), Ly6C (AL-21), CD11b (M1/70), and CD11c (N418) (eBioscience, San Diego, CA).

Statistics

Microarray results were normalized using RMA in the ‘affy’ package and differential expression p-values were calculated using the ‘limma’ package and adjusted for multiple comparisons by Benjamini-Hochberg procedure. All other data were analyzed by Student’s *t*

test or 2-way ANOVA and presented as mean ± SEM. Statistical analyses were performed using Prism software (version 5; GraphPad Software). *P* values less than 0.05 were considered significant.

Supplementary Material

Refer to Web version on PubMed Central for supplementary material.

Acknowledgments

We would like to thank Jennifer Pattison and Karen Bowden for their assistance with FPLC, lipid analysis and aortic root sectioning. We would also like to thank UCSD Histology core facility for assistance with histology and the UCSD hematology core facility for hematology analysis and Tiffany Lee for assistance with sample processing for qPCR analysis. This work was supported by NIH grant GM33063 and P01 HL107150 (to J.D. Esko), HL 088093 (to J.L. Witztum), HL30568 and HL28481 (to A.J. Lusis) and the European Community FP7 Award PIOF-GA-2010-273994 (to P.L.S.M. Gordts).

References

Abe M, Matsuda M, Kobayashi H, Miyata Y, Nakayama Y, Komuro R, Fukuhara A, Shimomura I. Effects of statins on adipose tissue inflammation: their inhibitory effect on MyD88-independent IRF3/IFN-beta pathway in macrophages. Arterioscler Thromb Vasc Biol. 2008; 28:871–877. [PubMed: 18323514]

Blich M, Golan A, Arvatz G, Sebbag A, Shafat I, Sabo E, Cohen-Kaplan V, Petcherski S, Avniel-Polak S, Eitan A, et al. Macrophage activation by heparanase is mediated by TLR-2 and TLR-4 and associates with plaque progression. Arterioscler Thromb Vasc Biol. 2013; 33:e56–e65. [PubMed: 23162016]

Boyanovsky BB, Shridas P, Simons M, van der Westhuyzen DR, Webb NR. Syndecan-4 mediates macrophage uptake of group V secretory phospholipase A2-modified LDL. J Lipid Res. 2009; 50:641–650. [PubMed: 19056705]

Clausen BE, Burkhardt C, Reith W, Renkawitz R, Forster I. Conditional gene targeting in macrophages and granulocytes using LysMcre mice. Transgenic Res. 1999; 8:265–277. [PubMed: 10621974]

de Weerd NA, Vivian JP, Nguyen TK, Mangan NE, Gould JA, Braniff SJ, Zaker-Tabrizi L, Fung KY, Forster SC, Beddoe T, et al. Structural basis of a unique interferon-beta signaling axis mediated via the receptor IFNAR1. Nat Immunol. 2013; 14:901–907. [PubMed: 23872679]

Dhoot GK, Gustafsson MK, Ai XB, Sun WT, Standiford DM, Emerson CP Jr. Regulation of Wnt signaling and embryo patterning by an extracellular sulfatase. Science. 2001; 293:1663–1666. [PubMed: 11533491]

Frank JS, Fogelman AM. Ultrastructure of the intima in WHHL and cholesterol-fed rabbit aortas prepared by ultra-rapid freezing and freeze-etching. J Lipid Res. 1989; 30:967–978. [PubMed: 2794795]

Goossens P, Gijbels MJ, Zernecke A, Eijgelaar W, Vergouwe MN, van der Made I, Vanderlocht J, Beckers L, Buurman WA, Daemen MJ, et al. Myeloid type I interferon signaling promotes atherosclerosis by stimulating macrophage recruitment to lesions. Cell Metab. 2010; 12:142–153. [PubMed: 20674859]

Gough DJ, Messina NL, Clarke CJ, Johnstone RW, Levy DE. Constitutive type I interferon modulates homeostatic balance through tonic signaling. Immunity. 2012; 36:166–174. [PubMed: 22365663]

Haka AS, Grosheva I, Chiang E, Buxbaum AR, Baird BA, Pierini LM, Maxfield FR. Macrophages create an acidic extracellular hydrolytic compartment to digest aggregated lipoproteins. Mol Biol Cell. 2009; 20:4932–4940. [PubMed: 19812252]

Hollmann W. Endurance training and the prevention of coronary heart disease. Boletin de la Asociacion Medica de Puerto Rico. 1989; 81:30–31. [PubMed: 2486904]

Jin C, Henao-Mejia J, Flavell RA. Innate immune receptors: key regulators of metabolic disease progression. Cell Metab. 2013; 17:873–882. [PubMed: 23747246]

Lawrence R, Olson SK, Steele RE, Wang L, Warrior R, Cummings RD, Esko JD. Evolutionary differences in glycosaminoglycan fine structure detected by quantitative glycan reductive isotope labeling. J Biol Chem. 2008; 283:33674–33684. [PubMed: 18818196]

MacArthur JM, Bishop JR, Wang L, Stanford KI, Bensadoun A, Witztum JL, Esko JD. Liver heparan sulfate proteoglycans mediate clearance of triglyceride-rich lipoproteins independently of LDL receptor family members. J Clin Invest. 2007; 117:153–164. [PubMed: 17200715]

Maor I, Hayek T, Hirsh M, Iancu TC, Aviram M. Macrophage-released proteoglycans enhance LDL aggregation: studies in aorta from apolipoprotein E-deficient mice. Atherosclerosis. 2000; 150:91–101. [PubMed: 10781639]

Moore KJ, Sheedy FJ, Fisher EA. Macrophages in atherosclerosis: a dynamic balance. Nat Rev Immunol. 2013; 13:709–721. [PubMed: 23995626]

Murata K, Murata A, Yoshida K. Heparan sulfate isomers in cerebral arteries of Japanese women with aging and with atherosclerosis--heparitinase and high-performance liquid chromatography determinations. Atherosclerosis. 1997; 132:9–17. [PubMed: 9247354]

Murphy AJ, Akhtari M, Tolani S, Pagler T, Bijl N, Kuo CL, Wang M, Sanson M, Abramowicz S, Welch C, et al. ApoE regulates hematopoietic stem cell proliferation, monocytosis, and monocyte accumulation in atherosclerotic lesions in mice. J Clin Invest. 2011; 121:4138–4149. [PubMed: 21968112]

Nakaya K, Tohyama J, Naik SU, Tanigawa H, MacPhee C, Billheimer JT, Rader DJ. Peroxisome proliferator-activated receptor-alpha activation promotes macrophage reverse cholesterol transport through a liver X receptor-dependent pathway. Arterioscler Thromb Vasc Biol. 2011; 31:1276–1282. [PubMed: 21441141]

Nardelli B, Zaritskaya L, Semenuk M, Cho YH, LaFleur DW, Shah D, Ullrich S, Girolomoni G, Albanesi C, Moore PA. Regulatory effect of IFN-kappa, a novel type I IFN, on cytokine production by cells of the innate immune system. J Immunol. 2002; 169:4822–4830. [PubMed: 12391192]

Osterholm C, Folkersen L, Lengquist M, Ponten F, Renne T, Li J, Hedin U. Increased expression of heparanase in symptomatic carotid atherosclerosis. Atherosclerosis. 2013; 226:67–73. [PubMed: 23137827]

Re F, Strominger JL. IL-10 released by concomitant TLR2 stimulation blocks the induction of a subset of Th1 cytokines that are specifically induced by TLR4 or TLR3 in human dendritic cells. J Immunol. 2004; 173:7548–7555. [PubMed: 15585882]

Robbins CS, Hilgendorf I, Weber GF, Theurl I, Iwamoto Y, Figueiredo JL, Gorbatov R, Sukhova GK, Gerhardt LM, Smyth D, et al. Local proliferation dominates lesional macrophage accumulation in atherosclerosis. Nat Med. 2013; 19:1166–1172. [PubMed: 23933982]

Sarrazin S, Lamanna WC, Esko JD. Heparan sulfate proteoglycans. Cold Spring Harb Perspect Biol. 2011; 3

Seimon TA, Obstfeld A, Moore KJ, Golenbock DT, Tabas I. Combinatorial pattern recognition receptor signaling alters the balance of life and death in macrophages. Proc Natl Acad Sci U S A. 2006; 103:19794–19799. [PubMed: 17167049]

Senda T, Saitoh S, Mitsui Y. Refined crystal structure of recombinant murine interferon-beta at 2.15 A resolution. J Mol Biol. 1995; 253:187–207. [PubMed: 7473712]

Shao C, Shi X, White M, Huang Y, Hartshorn K, Zaia J. Comparative glycomics of leukocyte glycosaminoglycans. Febs J. 2013; 280:2447–2461. [PubMed: 23480678]

Stanford KI, Bishop JR, Foley EM, Gonzales JC, Niesman IR, Witztum JL, Esko JD. Syndecan-1 is the primary heparan sulfate proteoglycan mediating hepatic clearance of triglyceride-rich lipoproteins in mice. J Clin Invest. 2009; 119:3236–3245. [PubMed: 19805913]

Swirski FK, Nahrendorf M. Leukocyte behavior in atherosclerosis, myocardial infarction, and heart failure. Science. 2013; 339:161–166. [PubMed: 23307733]

Tabas I, Williams KJ, Boren J. Subendothelial lipoprotein retention as the initiating process in atherosclerosis: update and therapeutic implications. Circulation. 2007; 116:1832–1844. [PubMed: 17938300]

Tacke F, Alvarez D, Kaplan TJ, Jakubzick C, Spanbroek R, Llodra J, Garin A, Liu J, Mack M, van Rooijen N, et al. Monocyte subsets differentially employ CCR2, CCR5, and CX3CR1 to accumulate within atherosclerotic plaques. J Clin Invest. 2007; 117:185–194. [PubMed: 17200718]

Tran-Lundmark K, Tran PK, Paulsson-Berne G, Friden V, Soininen R, Tryggvason K, Wight TN, Kinsella MG, Boren J, Hedin U. Heparan sulfate in perlecan promotes mouse atherosclerosis: roles in lipid permeability, lipid retention, and smooth muscle cell proliferation. Circ Res. 2008; 103:43–52. [PubMed: 18596265]

Viviano BL, Paine-Saunders S, Gasiunas N, Gallagher J, Saunders S. Domain-specific modification of heparan sulfate by Qsulf1 modulates the binding of the bone morphogenetic protein antagonist Noggin. J Biol Chem. 2004; 279:5604–5611. [PubMed: 14645250]

Wang XA, Zhang R, Zhang S, Deng S, Jiang D, Zhong J, Yang L, Wang T, Hong S, Guo S, et al. Interferon regulatory factor 7 deficiency prevents diet-induced obesity and insulin resistance. Am J Physiol Endocrinol Metab. 2013; 305:E485–E495. [PubMed: 23695216]

Wei W, Ninonuevo MR, Sharma A, Danan-Leon LM, Leary JA. A comprehensive compositional analysis of heparin/heparan sulfate-derived disaccharides from human serum. Anal Chem. 2011; 83:3703–3708. [PubMed: 21473642]

Wight TN. Cell biology of arterial proteoglycans. Arteriosclerosis. 1989; 9:1–20. [PubMed: 2643420]

Witztum JL, Lichtman AH. The influence of innate and adaptive immune responses on atherosclerosis. Annual review of pathology. 2014; 9:73–102.

Yang L, Yang JB, Chen J, Yu GY, Zhou P, Lei L, Wang ZZ, Cy Chang C, Yang XY, Chang TY, et al. Enhancement of human ACAT1 gene expression to promote the macrophage-derived foam cell formation by dexamethasone. Cell Res. 2004; 14:315–323. [PubMed: 15353128]

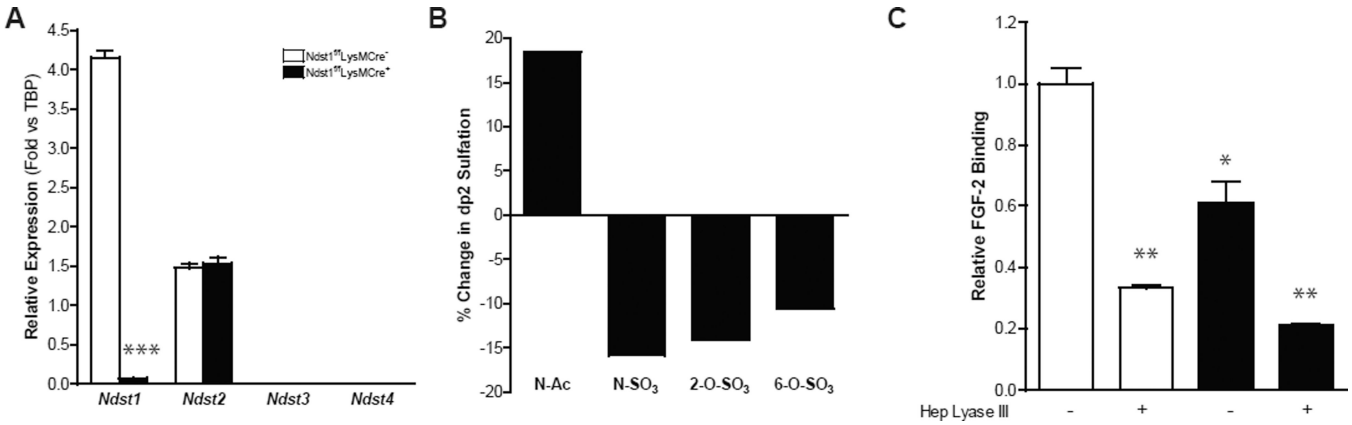

Figure 1. Characterization of *NDST1$^{f/f}$ LysMCre^{+}* Macrophages

(A) qPCR of *Ndst1-4* in Ndst1$^{f/f}$LysMCre^{+} and wild-type BMDMs (n = 3) (B) Changes in N-acetylated, N-sulfated, 2-O-sulfated and 6-O-sulfated HS disaccharide in Ndst1$^{f/f}$LysMCre^{+} BMDMs compared to wild-type BMDMs. (C) Relative FGF-2 binding in BMDMs treated or untreated with heparin lyase III (n = 2). Shown are mean values ± SEM, *p<0.05, **p<0.01 and ***p,0.001.

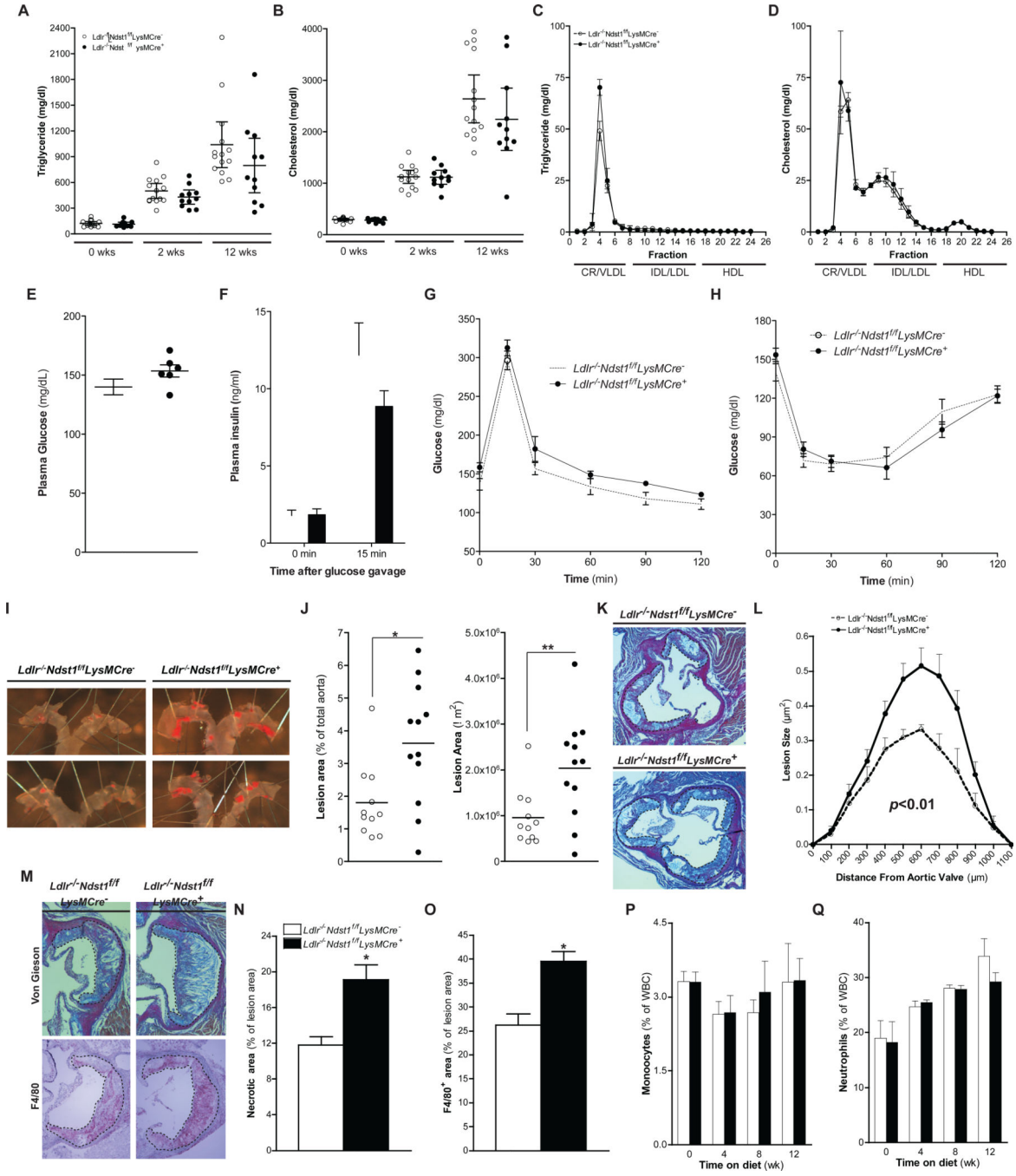

Figure 2. Macrophage *NDST1* Inactivation Increases Atherogenesis and Lesion Macrophage Content

Plasma cholesterol and triglycerides levels from female $Ldlr^{-/-}Ndst1^{f/f}$ and $Ldlr^{-/-}Ndst1^{f/f}LysMCre^{+}$ mice at different times after commencing HFC diet feeding (A and B). FPLC analysis of plasma after 12-weeks HFC diet feeding (n = 6) (C and D). Fasting plasma glucose and insulin levels before and after an oral glucose gavage (n=5–7) (E and F). Glucose tolerance (G) and insulin tolerance (G) tests were performed after 11-weeks HFC diet feeding (n=5–7). En face analysis of atherosclerosis and quantification of Sudan IV

positive area (E and F). Staining and quantification of atherosclerotic lesion size in the aortic sinus (n = 5–7) (G and H). Atherosclerotic lesions stained with Van Gieson for collagen or F4/80 for macrophages (I). Quantification of necrotic core size (J) and F4/80 positive area (K) in lesions after 12-weeks HFC diet feeding. Monocyte(L) and Neutrophil (L) counts in blood during HFC diet feeding. Shown are mean values ± SEM, *p<0.05 and **p<0.01.

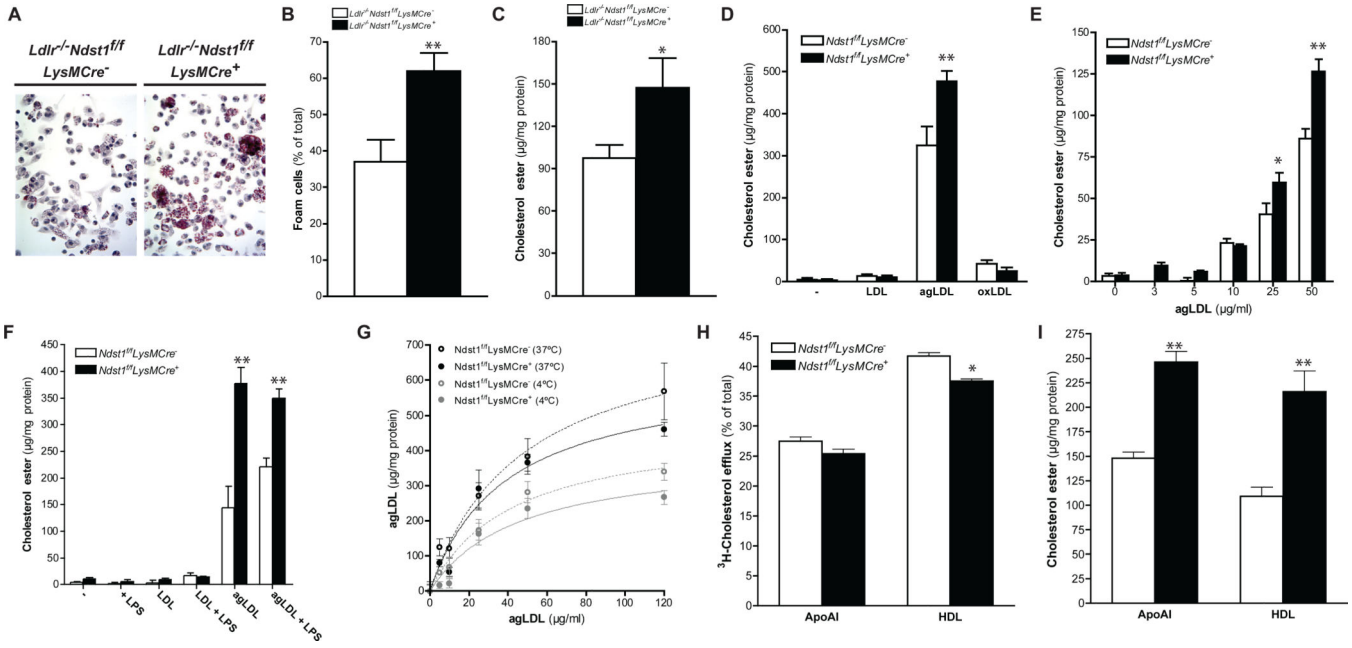

Figure 3. Macrophage *NDST1* Inactivation Increases Foam Cell Conversion

Oil Red O staining of peritoneal macrophages collected after 12-weeks HFC diet feeding (A). Oil Red O positive peritoneal macrophages (B) and cholesterol ester levels (C) in peritoneal macrophages collected after 12-weeks HFC diet feeding (n = 3/group). Cholesterol ester levels in BMDM after a 24h incubation with 0 or 50 µg/ml of LDL, agLDL and oxLDL (n = 3) (D). Cholesterol ester levels in BMDM after a 24h incubation with different concentrations of agLDL (n = 3) (E). Cholesterol ester levels in BMDM after a 24h incubation with 0 or 50 µg/ml of LDL and agLDL in the presence or absence of 100 ng/ml LPS (n = 3) (F). Binding at 4°C or uptake at 37°C for 1h of DiD-agLDL in BMDMs (n = 3) (G). Cholesterol efflux in BMDMs after 24h incubation with 10 µg/ml apoAI or 50 µg/ml HDL (n = 3) (H). Cholesterol ester content in BMDMs after cholesterol efflux with 10 µg/ml apoAI or 50 µg/ml HDL (n = 3) (I). Shown are mean ± SEM, *p<0.05 and **p<0.01.

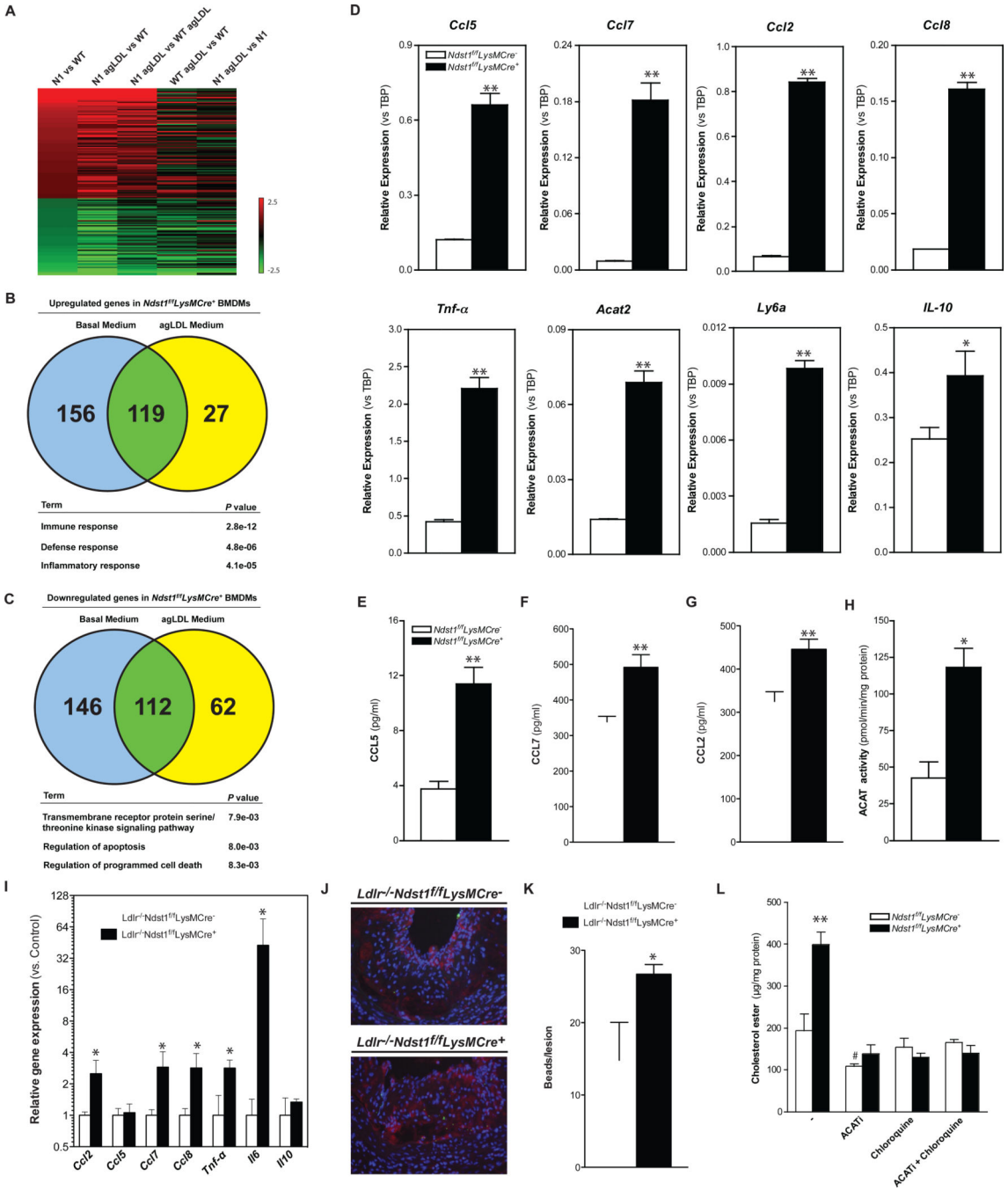

Figure 4. Reducing Macrophage HSPG Sulfation Increases Expression of Inflammatory Genes

Microarray analysis on RNA isolated from BMDMs (n = 4/group). Gene expression was filtered for genes from untreated Ndst1$^{f/f}$LysMCre^{+} BMDMs at least 2-fold different from WT control (A). Venn diagram of > 1.5x upregulated genes (B) and < 1.5x downregulated genes (C) and their overlap by agLDL treatment in the transcriptome of wild-type and Ndst1$^{f/f}$LysMCre^{+} BMDMs, and p values for selected gene ontology (GO) terms. qPCR validation from WT and Ndst1$^{f/f}$LysMCre^{+} BMDMs (D–F). Secretion of CCL5, CCL2 and CCL7 in the media by BMDMs after 24h at 37°C (E–G). ACAT activity levels in cell

lysates from WT and Ndst1$^{f/f}$LysMCre^{+} BMDMs (H). qPCR validation from atherosclerotic plaques isolated from *Ldlr* $^{-/-}$ *Ndst1*$^{f/f}$*LysMCre* $^{-}$ and *Ldlr* $^{-/-}$ *Ndst1*$^{f/f}$*LysMCre* $^{+}$ mice after 12-weeks HFC diet feeding.(n=3–4) (I). Micro-images and quantification of infiltrated fluorescent bead-labeled Ly6C high monocytes (green) in lesions of *Ldlr* $^{-/-}$ *Ndst1*$^{f/f}$*LysMCre* $^{+}$ mice. Atherosclerotic lesions were stained for CD68 positive macrophages (red) and with DAPI for nuclei (blue) (n=3/group) (J–K). Cholesterol ester levels in BMDM after a 24h incubation with 50 μg/ml agLDL in the presence or absence of 10 μg/ml Sandoz 58–035 (ACATi), 30μM chloroquine or a combination (n = 3) (L). Shown are mean values ± SEM, *p<0.05 and **p<0.01.

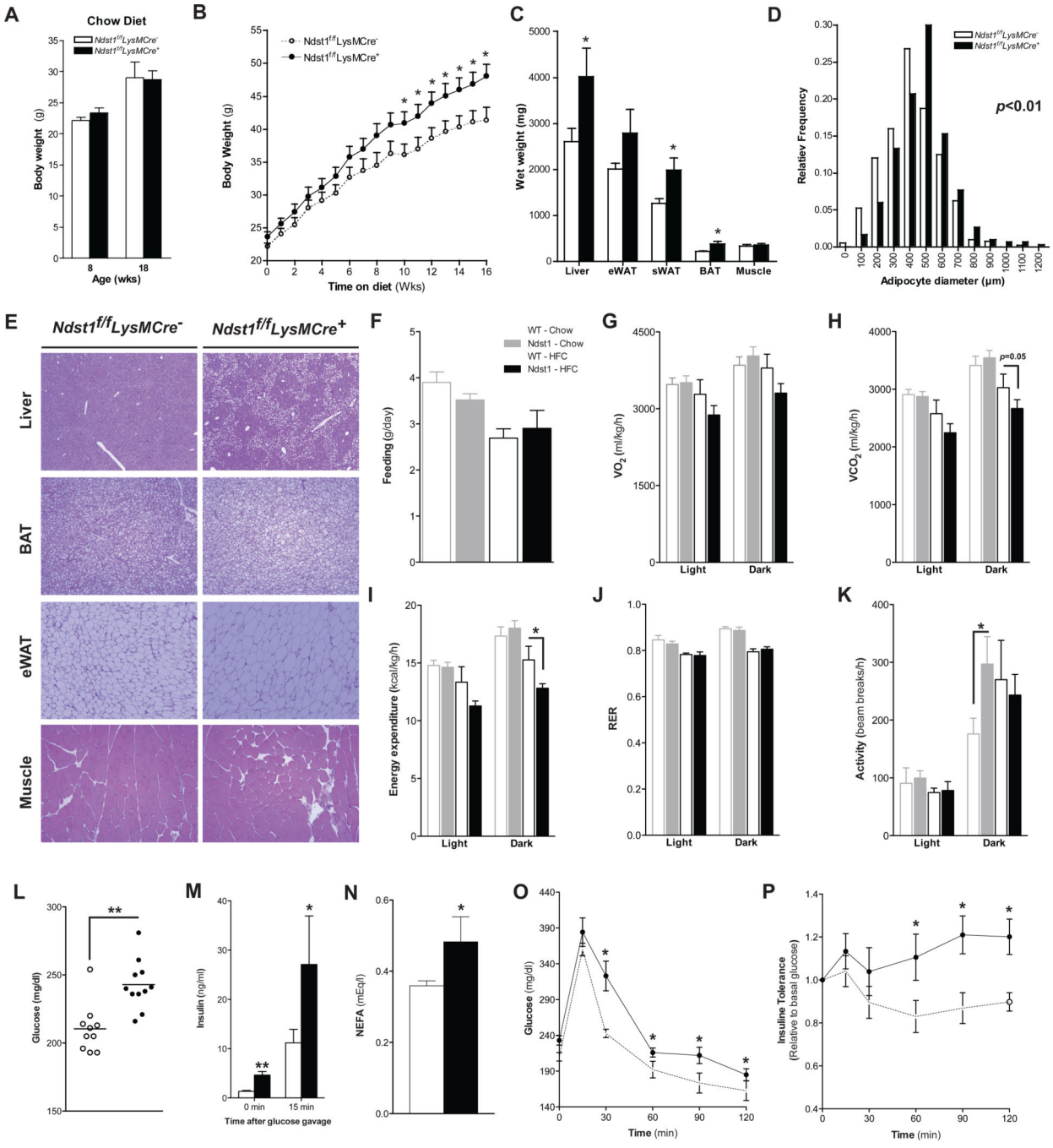

Figure 5. Reducing Macrophage HSPG Sulfation Promotes Diet-Induced Obesity

Body weights of 8- and 18-weeks old male Ndstf$^{f/f}$LysMCre- and Ndst1$^{f/f}$LysMCre^{+} mice on a chow diet (n = 4–8) (A). Male Ndstf$^{f/f}$LysMCre- and Ndst1$^{f/f}$LysMCre^{+} mice on a HFC diet were weighed weekly (n = 8–10) (B). Wet weights of the liver, eWAT, sWAT, BAT and biceps femoris muscle after 18-weeks on the HFC diet (C). Adipocyte diameter distribution in eWAT (D) and H&E staining of Liver, eWAT, sWAT, BAT and biceps femoris muscle (E) of Ndst1$^{f/f}$LysMCre and Ndst1$^{f/f}$LysMCre^{+} mice 18-weeks on a HFC diet (n = 4/group). Feeding behavior of 26-week old *Ndst1$^{f/f}$LysMCre* $^{-}$ and

Ndst1$^{f/f}$*LysMCre* $^{+}$ on a chow or HFC diet for 18 weeks (n = 4–6) (F). Average VO_2 (ml/kg/hr) (G) and average VCO_2 (H) in the light and dark cycles. Energy Expenditure (I) and Respiratory Exchange Ratio (RER) (J) in *Ndst1*$^{f/f}$*LysMCre* $^{-}$and *Ndst1*$^{f/f}$*LysMCre* $^{+}$mice littermates over a 24-hour period. Average activity in the dark and light cycles (K). Fasting plasma glucose levels (L), fasting NEFA levels (M) and insulin levels before and 15 min after an oral glucose gavage (N) in *Ndst1*$^{f/f}$*LysMCre* $^{-}$ and *Ndst1*$^{f/f}$*LysMCre* $^{+}$ mice on a HFC diet (n = 4–6). (O) Glucose tolerance and insulin tolerance (P) tests were performed after 16-weeks on a HFC diet (n = 9). Shown are mean ± SEM, *$p<0.05$ and **$p<0.01$.

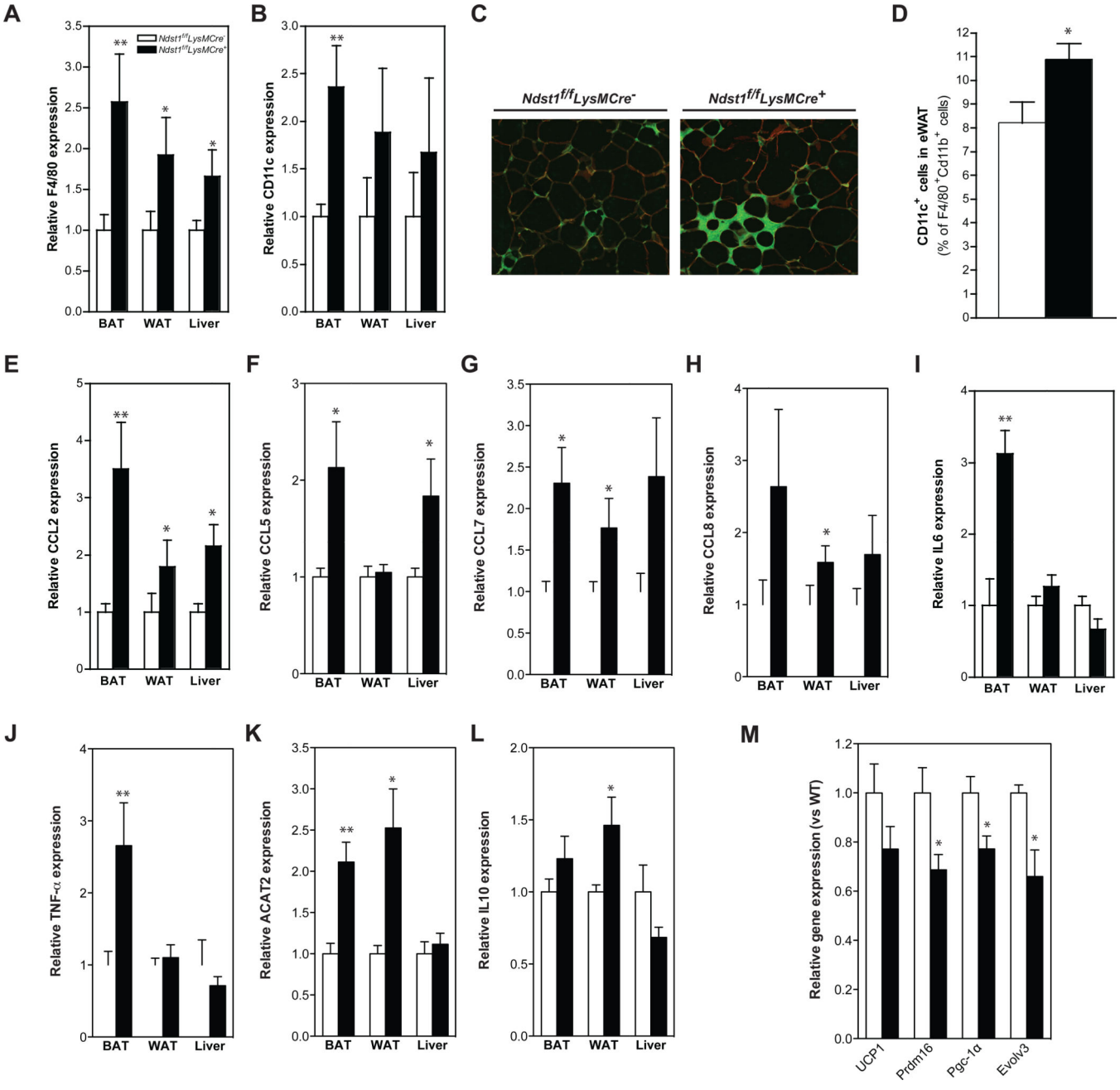

Figure 6. Macrophage HSPGs regulate adipose tissue inflammation in a model of diet-induced obesity

Expression of F4/80 and CD11c in BAT, eWAT and liver after 18-weeks on a HFC diet (A–B). Immunostaining images from eWAT of HFD-fed *Ndst1$^{f/f}$LysMCre* $^{-}$ and *Ndst1$^{f/f}$LysMCre* $^{+}$ mice co-stained with anti-F4/80 (green) and anti-caveolin-1 (red) antibodies (C). FACS analysis of F4/80+/CD11b+/CD11c+ cells in stromal vascular cells (n4–5/group) (D). Expression of CCL2, CCL5, CCL7, CCL8, IL6, TNF-a and IL10 in BAT, eWAT and liver after 18-weeks on a HFC diet (E–K). Expression of UCP1, Prdm16, Pgc-1α and Evolv3 in BAT liver after 18-weeks on a HFC diet (n = 4– 5/group) (L). Shown are mean values ± SEM, *p<0.05 and **p<0.01.

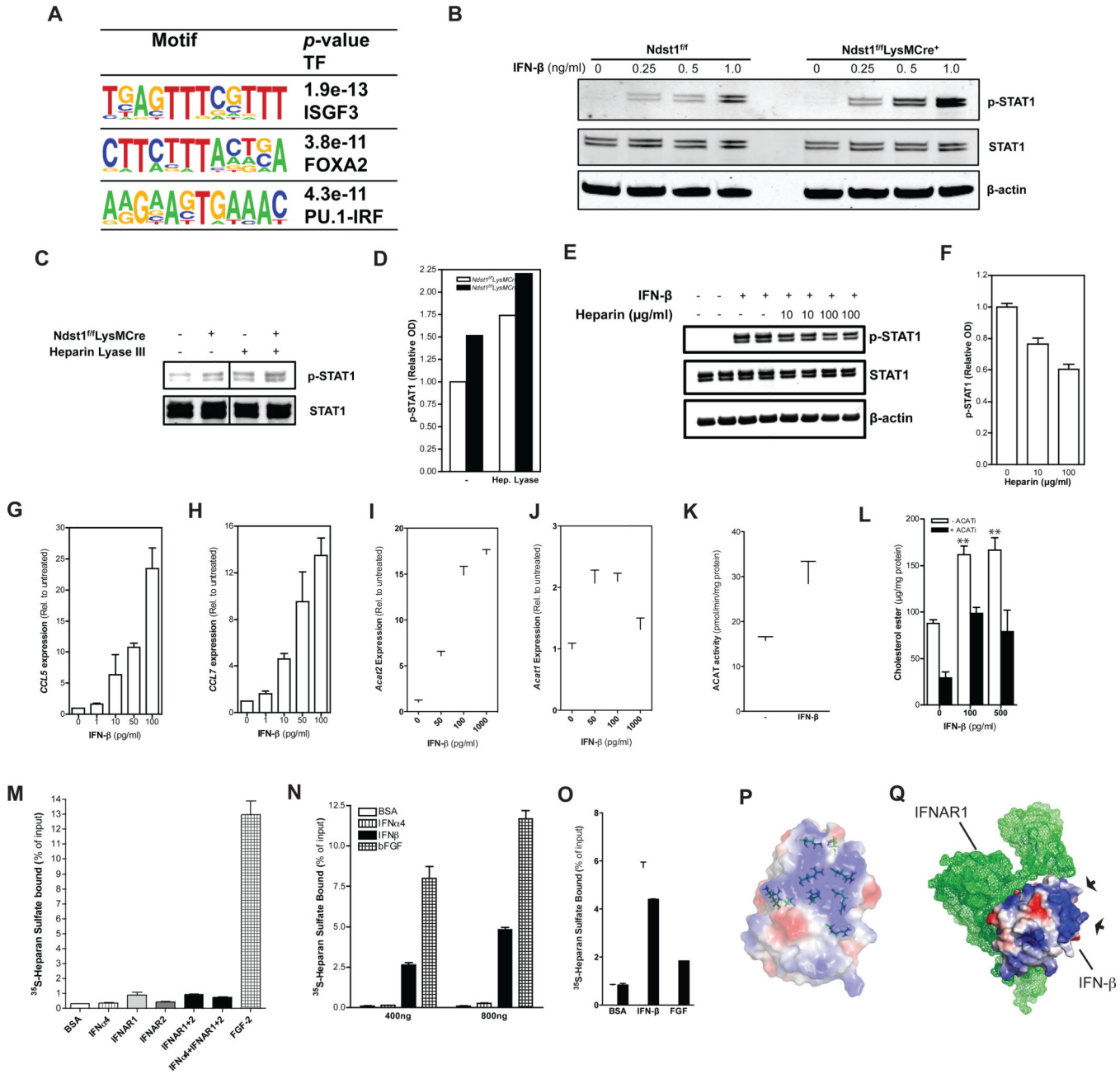

Figure 7. Macrophage HSPGs Regulate Type I Interferon Signaling

Sequence motifs identified by de novo motif analysis of the promoters of upregulated genes in Ndst1$^{f/f}$LysMCre^{+} BMDMs (>1.5 x from WT) (A). Immunoblot analysis of STAT1, phosphoSTAT1 (pSTAT1) and β-actin in BMDMs after stimulation with different concentrations of IFN-β for 30 min (B). Immunoblot analysis and quantification of STAT1 and phosphoSTAT1 (pSTAT1) in BMDMs after stimulation with 0.5 ng/ml IFN-β for 30 min. Cells were preincubated with or without Heparin Lyase III at 5 mU/mL for 20 min prior to stimulation (C–D). Immunoblot analysis and quantification of STAT1 and phosphoSTAT1 (pSTAT1) in WT BMDMs after stimulation with 5 ng/ml IFN-β for 30 min and co-incubated with 0, 10 or 100 μg/ml heparin (E–F). qPCR of CCL5 and CCL7 from

WT and Ndst1$^{f/f}$LysMCre^{+} BMDMs after stimulation with different concentrations of IFN-β for 4 hr (G–H). qPCR of ACAT2 and ACAT1 from wild-type and *Ndst1$^{f/f}$LysMCre* $^{+}$BMDMs after stimulation with different concentrations of IFN-β for 24 hr (I–J). ACAT activity in BMDMs stimulated with or without rmIFN-β for 24 hr (K). Cholesterol ester levels in BDMDs stimulated with or without rmIFN-β for 24 hr after an additional 24 hr incubation with 50 μg/ml agLDL in the presence or absence of 10 μg/ml Sandoz 58–035 (ACATi) (L). Binding of BSA, IFNAR-1, IFNAR-2, IFNα4, a combination of IFNa4, IFNAR-1 and IFNAR-2, and FGF2 to ^{35}S-labeled HS obtained from wild-type BDMDs as determined by filter binding assay (n = 3) (M). Dose-dependent binding of BSA, IFN-β, IFNa4 and FGF2 to ^{35}S-labeled macrophage HS as determined by filter binding assay (n = 2) (N). Binding of BSA, IFN-β or FGF2 (600 ng) to ^{35}S-labeled macrophage HS obtained from either wild-type or and *Ndst1$^{f/f}$LysMCre* $^{+}$ BMDMs as determined by filter binding assay (O). A schematic representation of a crystal structure of murine IFN-β (Protein Data Bank code 1WU3). Charge distribution at the protein surface is shown (red is negatively and blue is positively charged) (P). Schematic representation of the crystal structure of murine IFNAR1 (green mesh) in complex with IFN-β (Protein Data Bank code 3WCY). Arrows indicate arginine-rich patch on IFN-β (Q). Shown are mean values ± SEM, **p<0.01.